Evidence of direct optical transitions in γ-In2Se3

Lola de Brucker, Wilfried Desrat, Matthieu Moret, Bernard Gil

Evidence of direct optical transitions in γ-In_2Se_3

L. de Brucker[1], M. Moret[1], B. Gil[1], W. Desrat[1]
[1] *Laboratoire Charles Coulomb (L2C), Université de Montpellier, CNRS, Montpellier, FR-34095, France*
(Dated: October 12, 2024)

We present an optical study of high cristalline quality γ-In_2Se_3 films grown epitaxially on (0001)-oriented sapphire. Well-defined structures are detected at 2.147 eV, 2.240 eV, 2.359 eV and 2.508 eV in the optical absorption at $T = 10$ K. On the basis of the selection rules, we associate them to direct optical transitions with excitons built from the upper and spin-orbit split off valence bands and the first conduction band at the Γ point. The first two lowest excitonic peaks vanish from the absorption spectrum above $T = 120$ K at a critical temperature for which the photoluminescence emission fades out as well. It leads us to an estimate of the exciton binding energy of the order of 10 meV in γ-In_2Se_3. Last we interpret additional absorption peaks to LO-phonon replicas of the free exciton with a phonon energy of ~ 14 meV.

I. INTRODUCTION

The van der Wals (vdW) materials are about to revolutionize the opto-electronic components due to their two dimensional (2D) nature that offers a complete freedom to model tailor-made ultrathin heterolayer-based devices. Their outstanding intrinsic properties promise significant advances in semiconductor applications based on valleytronics, twistronics or straintronics [1–3]. More specifically, the physics of the ferroelectricity is boosted in vdW layered compounds with unprecedented mechanisms like the polar stabilization or the switching kinetics, which are reviewed exhaustively in Ref. [4]. One of the spearhead of these materials is α-In_2Se_3 which reveals non-zero in-plane (IP) and out-of-plane (OOP) polarizations at room temperature, as well as a coupling between both components, known as the dipole locking effect, where the switching of one dipole reverses the second one [5–7]. The recent discovery of these unusual properties, i.e. the stability and switchability of the polarization at room temperature, has generated a vast research on the 2H and 3R polymorphs of α-In_2Se_3 [8], from which the ferroelectricity arises due to the non-centrosymmetric cristalline structure of the vdW-stacked layers. A recent study reports that γ-In_2Se_3 films, which have not a 2D structure, exhibit also IP and OOP at $T = 300$ K [9]. Therefore the research devoted to the enhancement of the crystalline quality of In_2Se_3 thin films has to be pursued for a finer determination of the polarization properties of the different polytypes of In_2Se_3. Additionally most of the ferroelectric field effect transistors are currently fabricated manually from the exfoliation of bulk samples [10, 11]. As a consequence the epitaxy of In_2Se_3 must be developed since a good knowledge of the growth will also enable the large scale production of more complex devices such as multiferroic tunnel junctions [12] and will allow the synthesis of In_2Se_3-based heterojunctions [13, 14], in which the OOP polarization will play a predominant role at the interface.

Historically the γ-polymorph has attracted attention among the other polytypes of In_2Se_3 due to its higher bandgap, of the order of 2 eV at room temperature which makes it fairly suitable for photovoltaic applications [15]. It has been used as a buffer layer in Mo/CuInSe/In_2Se_3/ZnO solar cells [16] or as a first growth step in a CuInSe absorber before the copper diffusion [17]. This material is potentially interesting for indoor photovoltaics as well, which focusses on the light wavelengths in the visible rather than on the broadband infrared contribution of the solar light spectrum. Like many vdW compounds, the bandgap of γ-In_2Se_3 depends on the number of stacked layers and increases up to 2.5 eV when the film thickness slims down to the monolayer [18].

Bulk crystals of γ-In_2Se_3 have first been grown by chemical vapor transport in sealed ampoules [18–21]. Single-source and double-source metal organic chemical vapor deposition (MOCVD) processes have also been extensively studied to produce thin films [22–24]. The main precursors are H_2Se for the chalcogen source and dimethyl- or trimethyl-indium for the element III [25]. Here we focus on the co-evaporation of γ-In_2Se_3 films from indium and selenium sources [15, 26, 27]. We report the growth of good cristalline quality γ-In_2Se_3 epitaxial films on (0001)-oriented sapphire wafers, which exhibit remarkable optical absorption spectra.

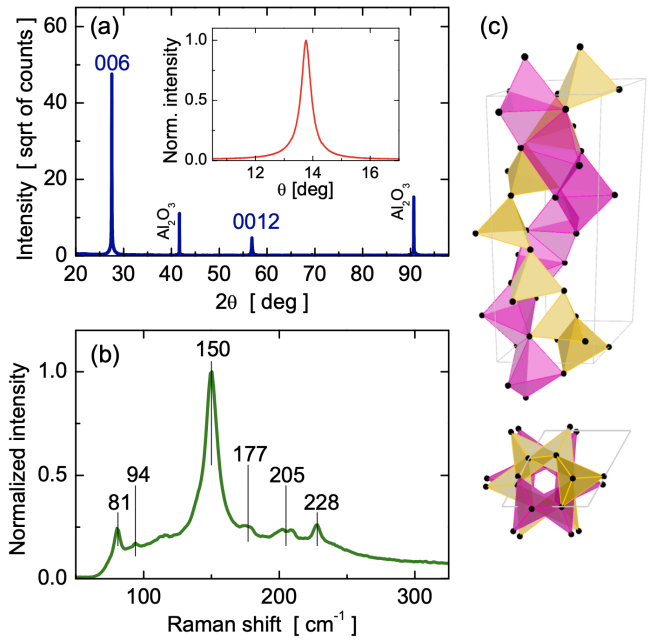

FIG. 1. (a) $\theta - 2\theta$ x-ray diffractogram of a γ-In_2Se_3 film grown on (0001)-oriented sapphire substrate. The unit of the XRD intensity is the square root of counts per second. The rocking curve of the main (006) peak is plotted in inset. (b) The room temperature Raman spectrum of a γ-In_2Se_3 film. The thin vertical lines indicate the energies of the vibrational modes. (c) The helical structure of the crystal cell in side and in top view. The black dots represent the selenium atoms.

II. EPITAXY OF γ-IN_2SE_3 FILMS

The γ-In_2Se_3 films have been epitaxially grown by co-evaporation on (0001)-oriented sapphire substrates in ultra-high vacuum. The temperature of the indium effusion cell is set at $T_{In} = 790\,°C$, which leads to an average growth rate of 500 nm/h. The temperature of the selenium source T_{Se} is tuned in such a way that the ratio of the beam equivalent partial pressures of the VI/III elements is optimized to target the In_2Se_3 stoechiometry as checked by energy dispersive x-ray spectroscopy. Our optimum growth parameters are $T_{Se} = 195 - 197\,°C$ and a temperature substrate equal to $T_s = 450\,°C$. It is consistent with the previous studies, which have demonstrated that a sufficient provision of selenium is required for the growth of the selenium-rich phase In_2Se_3 [15, 26–28]. Depending on the growth set-ups, the formation of this phase occurs for values of the Se/In beams ratio R ranging from 2, similar to our conditions, up to 10. Recently the synthesis of the β polymorph of In_2Se_3 was reported by molecular beam epitaxy (MBE) for higher T_s and higher values of R [29].

Figure 1(a) shows the $\theta - 2\theta$ x-ray diffractogram of a γ-In_2Se_3 film, which highlights the preferential orientation of the $(00l)$ planes of the crystallites along the (0001) direction of the sapphire substrate. The detection of the main (006) and (00 12) peaks at 27.532° and 56.837° respectively leads to a c lattice parameter of the hexagonal cell equal to 19.42 $\AA$. This is slightly larger than the usual value of 19.38 $\AA$ reported for the bulk by only 0.2 % [21, 30]. However it was demonstrated in Ref. [27], that the c parameter could be dependent on the growth temperature of the soda lime glass substrates spanning from 19.38 $\AA$ up to 19.44 $\AA$. The formation of grains of a metastable phase competing with the γ-phase which induces constraints along the c axis during the growth was suggested for interpreting this observation. Besides, the in-plane lattice parameter a was measured constant in an identical way to what we observe with a value of $a = 7.12$ $\AA$, in perfect agreement with the bulk value [19, 21]. The crystallite size along the growth direction is estimated of the order of 150 nm from a simple Debye-Scherrer analysis of the main diffraction peak.

The growth of γ-In_2Se_3 on crystalline sapphire wafers favors the orientation of the layers and reduces the mosaicity in contrast to the observation reported in the case of the deposition on amorphous glass substrates. The inset of Fig. 1(a) displays the rocking curve of the (006) main peak, whose full width at half maximum is of the order of 0.4°. It remains significant and results from the misorientations of the cristallites out of the c-axis of sapphire. It is comparable to the value of 0.55° recently reported for γ-In_2Se_3 films deposited by MBE on mica [31]. Thus, our epitaxial γ-In_2Se_3 layers grown by co-evaporation are of good crystalline quality, which will be confirmed by the optical results presented below. The γ phase unlike the other polymorphs of In_2Se_3 (α, β, ...) is not a 2D layered material and therefore follows more stringent conditions in terms of lattice matching with the substrate than for van der Waals epitaxy. Thus the nature of the substrate material is likely the main origin of the present crystallographic quality limitations of our In_2Se_3 films. By the way, the existence of a turbostratic-like stacking which occurs sometimes in 2D compounds, like in boron nitride or graphite [32, 33], is ruled out to explain the larger c lattice parameter in our epilayers. The absence of distinct atomic sheets is visible from the 3D crystallographic structure sketched in Fig. 1(c) based on a distorted wurtzite lattice. It is formed by two inter-

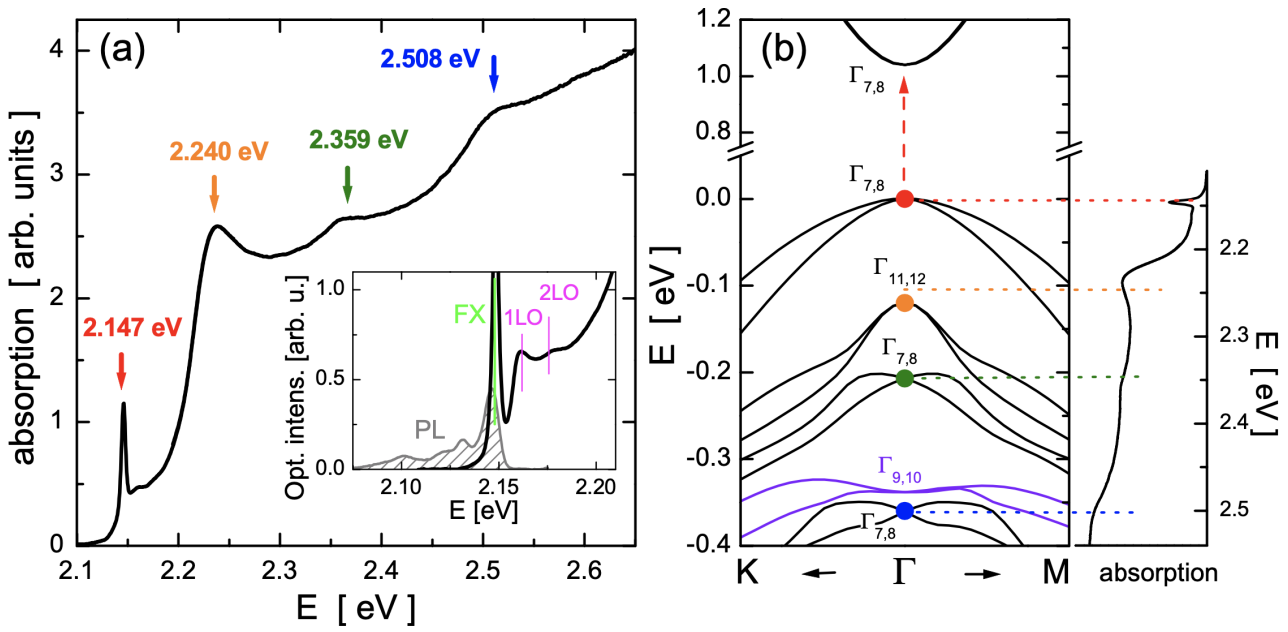

FIG. 2. (a) Optical absorption of a γ-In_2Se_3 film at $T = 10$ K. The arrows highlight distinct features in the absorption curve. The inset focusses on the band edge region with the photoluminescence (gray) and absorption spectra (black). (b) Band diagram of γ-In_2Se_3 around the Γ point along the $K - \Gamma - M$ path in the Brillouin zone. The vertical arrow represents an allowed direct optical transition from the upper valence band to the lowest conduction band at $k = 0$. The colors of the dots and the horizontal lines match with the colors of the arrows in Fig. 1(a).

twined screws made of a chain of tetrahedra connected by a common corner and a chain of bipyramids (octahedra) linked by an edge [21]. Selenium and indium atoms are respectively at the corners and in the centers of these polyhedra. Interestingly, from this helical shape, it results a large optical rotary power in γ-In_2Se_3 [28].

The crystalline quality of our films is further demonstrated by Raman spectroscopy. Figure 1(c) shows the typical Raman spectrum of a γ-In_2Se_3 sample measured in backscattering configuration at room temperature with a laser wavelength of 473 nm. The high-frequency modes at 81, 94, 150, 177, 205 and 228 cm^{-1} are the clear signatures of the γ-polymorph with the prominent peak at 150 cm^{-1} [34, 35]. In addition, these experimental values are compared with the computed energies of the vibrational modes, listed in the Supplemental Material [**?**].

III. EXCITONS AND PHONON ASSISTED ABSORPTION PROCESSES AT LOW ENERGIES

Figure 2(a) presents the main result of this paper, namely the low temperature optical absorption of a representative γ-In_2Se_3 film. The data is reproducible. It has been recorded on 4 different samples grown with slightly different conditions. A first sharp peak is detected at 2.147 eV close to the absorption edge, followed by successive steps at higher energies (2.240, 2.359 and 2.508 eV) indicated by vertical arrows. An additional plateau at 2.700 eV has to be confirmed. The interaction of the high energy excitons with the lowest continuum of states broadens them. We suggest that these features are due to direct photon absorption at Γ (i.e., at the center of the Brillouin zone) from the top and the lower spin orbit split-off valence bands to the first conduction band, as represented in Fig. 2(b) [36].

First we focus on the close vicinity of the bandgap where the absorption curve reveals 3 peaks at $T = 10$ K (see inset of Fig. 2(a)). The main peak at $E = 2.147$ eV is undoubtedly the signature of the free exciton (FX), i.e. the $n = 1$ exciton. It was reported previously for polycrystalline γ-In_2Se_3 but the experimental data was not shown [28]. The second peak at 2.161 eV, 14 meV above, may be attributed to the $n = 2$ exciton. The third one at 2.177 eV is much broader and looks like the "hump" reported in several semiconductors, like InSe [37, 38]. In the present case, it is obvious that the latter cannot correspond to the $n = 3$ exciton. Indeed from the energies of

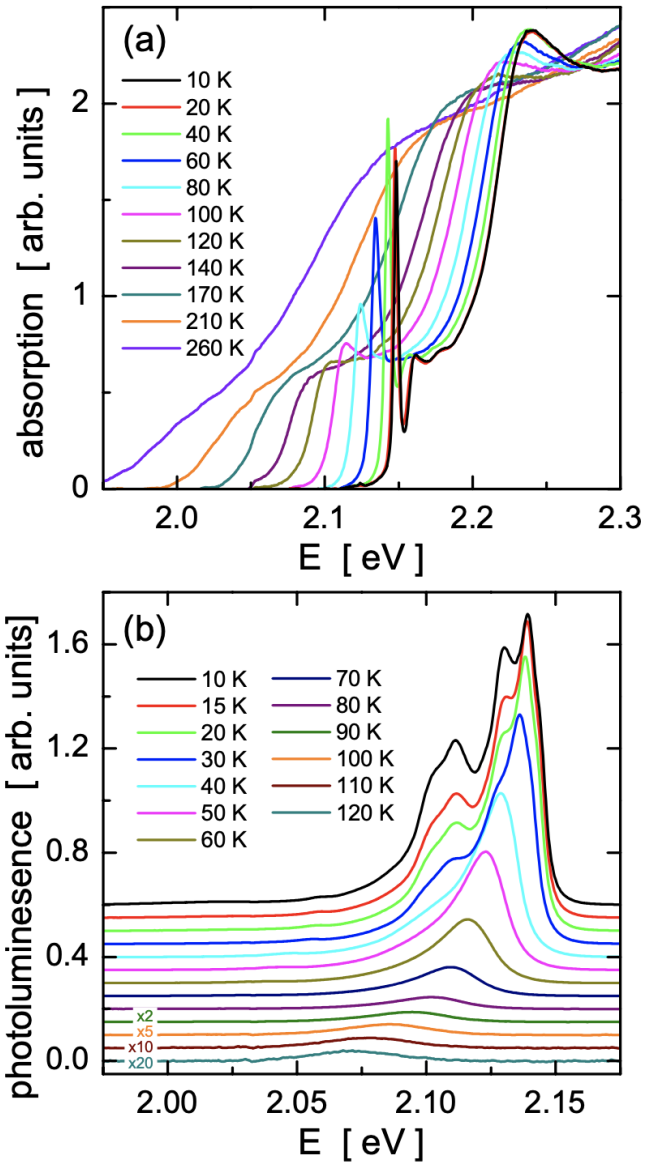

FIG. 3. Temperature dependence of the absorption (a) and photoluminescence (b) spectra of γ-In_2Se_3.

the $n = 1$ and supposed $n = 2$ peaks one would obtain an exciton binding energy of 19 meV and a $1s - 3s$ splitting of 16.9 meV. The bandgap should therefore be located at 2.166 eV, that is to say below the energy of the hump. Also the 2.161 eV line presents an excessive broadening compared to the width of the 2.147 eV peak. Nothing pleads for this observation in the theory of the dielectric function [39]. Among different origins (3D Sommerfeld factor, interband matrix element, ...), the most plausible explanation of the side peak is a longitudinal optical (LO) phonon replica of the $n = 1$ excitonic peak, in a similar way to what occurs in II-VI materials [40], other monochalcogenides [41] and wurtzitic nitrides [42, 43]. In a 1-LO phonon process the phonon energy would be equal to 30 meV. If a 2-LO phonon process is assumed the second peak, first attributed to the $n = 2$ exciton and located at half energy (i.e. ~ 14 meV), could be associated to the 1-LO phonon replica. The optical reflectivity data displayed in the Supplemental Material supports this identification [**?**]. The reexamination and our proposal of this peak are supported by the questionable large value of the Rydberg, since the FX peak disappears completely in the optical absorption spectra above $T = 120$ K (Fig. 3(a)). The photoluminescence (PL) emission vanishes at the same temperature as well (Fig. 3(b)) and therefore suggests an exciton binding energy of the order of 10 meV. Hence the interpretation of the 2.161 eV and 2.177 eV peaks in terms of the 1-LO and 2-LO replica of the $n = 1$ excitonic peak makes sense. The polar phonon of 120 cm^{-1}, i.e. 15 meV, present in the list of the vibrational modes in the Supplemental Material [**?**], can account for this energy difference. The second phonon-assisted feature is smoother and broader than the first one, which is also coherent with our interpretation.

From the temperature dependence of the energy of the FX peak, which is plotted in Fig. 4(a) we can assert that the zero temperature bandgap of γ-In_2Se_3 equals $E_g(0) \approx 2.15$ eV in this sample, in agreement with the value reported in Ref. [28]. The gap value comes up to 2.16 eV in other samples (see Supplemental Material [**?**]). The dependence of the full width at half maximum (FWHM) of the $n = 1$ peak is traced as a function of T in Fig. 4(b). The fit by the exciton broadening function $\Gamma(T) = \Gamma(0) + \beta/[\exp(\hbar\omega_{ph}/k_BT) - 1]$ leads to a zero broadening $\Gamma(0) = 3.7$ meV for the FX absorption peak, an electron-optical phonon coupling constant $\beta = 157$ meV and an average phonon energy of 21 meV. The latter is found equal to 17 meV from the PL data. The acoustic phonon contribution proportional to T remains negligible.

The photoluminescence was measured as a function of temperature with a Q-switched green laser of 532 nm. The low temperature traces in Fig. 3(b) show a response composed of several peaks as described earlier [44]. The high energy peak is the free exciton since its energy corresponds to the one of the $n = 1$ absorption peak Stokes-shifted of about 1 meV at the lowest excitation power (see inset in Fig. 2(a)). The adjacent peaks were attributed to bound excitons in the past, but phonon replicas could be now considered, as the separation between the two

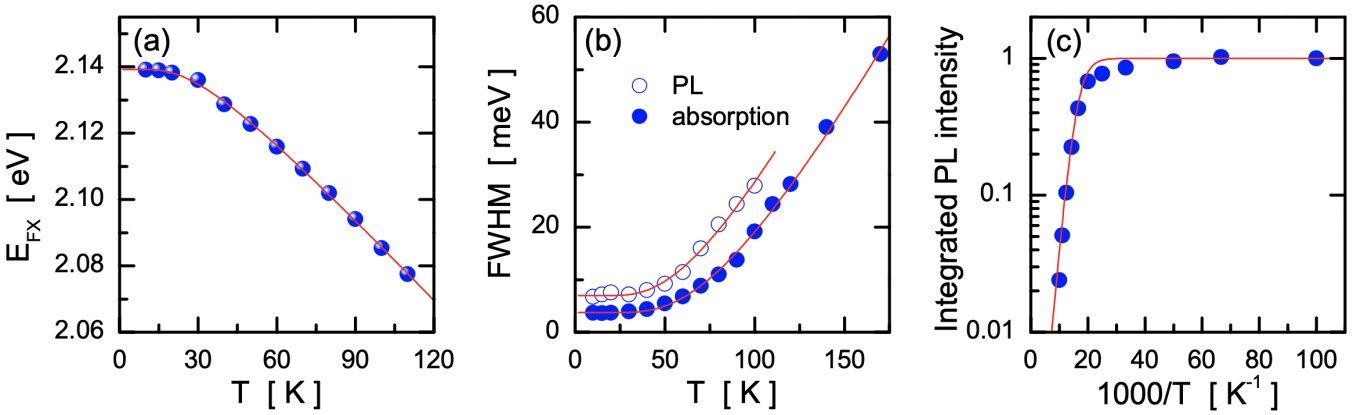

FIG. 4. (a) Energy of the free exciton (FX) peak detected in the absorption vs temperature. (b) Full width at half maximum of the FX peak vs temperature measured from the absorption (dots) and the PL spectra (open circles). (c) Arrhenius plot of the integrated whole PL spectrum vs $1000/T$. The solid line is the fit by the single recombination process discussed in the text.

highest peaks is ~ 14 meV. The PL signal is completely quenched above $T \approx 120$ K whatever the laser power. This behavior was previously reported in Refs. [24, 45], while some authors observed the persistence of the PL signal up to room temperature [46, 47]. It reveals the predominance of the excitonic emission, without the noticeable detection of deep defects at low T, and of the non radiative emission at high temperature. The Arrhenius plot of the integrated PL peak intensity is plotted vs $1000/T$ in Fig. 4(c). The data is fitted by a single channel recombination process:

$$I(T) = \frac{I_0}{1 + AT^{\frac{3}{2}} \exp(-E_a/k_B T)} \qquad (1)$$

where the $T^{3/2}$ dependence accounts for the effective density of the band continuum states [48]. The activation energy $E_a \approx 30$ meV is in good agreement with the previous reported values between 25 meV and 41 meV [17, 24, 46].

IV. BANDS SYMMETRY AND OPTICAL SELECTION RULES

The low temperature absorption curve presents several steps in the band to band region far from the bandgap (Fig. 2(a)). A second absorption edge is detected at 2.240 eV, with a fairly broad excitonic peak that fades out with increasing temperature (Fig. 3(a)). This situation can be compared qualitatively to what happens in InSe with optical transitions from the p_z-like topmost and lower p_x, p_y-like spin-orbit split off valence bands (VB) to the lowest s-like conduction band (CB) [37, 49, 50]. In the present case, additional steps at 2.359 eV and 2.508 eV are detected. We attribute all these features to direct transitions at $k = 0$ from the upper and subjacent valence bands to the lowest conduction band. The computed band dispersion is shown in the vicinity of the Γ point in Fig. 2(b) (computational details are given in the Supplemental Material [**?**]). The value of the bandgap (~ 1.05 eV) is far from the experimental value which is inherent to the band computation within the generalized gradient approximation. However the second CB is located approximately 600 meV above the first CB (see Fig.2 in the Supplemental Material [**?**]), while the splittings between the successive VBs are smaller and equal 122, 87 and 132 meV, from top to bottom VBs. They are in agreement with the 93, 119 and 149 meV splittings measured experimentally between each kink in the absorption curve. Here we consider that the incorrect underestimated bandgap does not alter significantly the dispersion and the energies of the valence bands at Γ, which supposes a rigid shift of the bands. Of course a better match could certainly be obtained between the experimental and the theoretical values after an optimized calculation of the bands dispersion. Taking the spin-orbit coupling into consideration allowed a rather good agreement with the observed valence band splittings.

Now we examine the symmetry of the bands to check if the selection rules allow the suggested optical transitions.

The minimum of the conduction band at Γ transforms like $\Gamma_7 + \Gamma_8$ according to the notations used in Ref. [51] that we adopt here. Regarding the valence band at Γ, the first five successive states transform like $\Gamma_7+\Gamma_8$, $\Gamma_{11}+\Gamma_{12}$, $\Gamma_7+\Gamma_8$, $\Gamma_9+\Gamma_{10}$, and $\Gamma_7+\Gamma_8$, in terms of increasing hole energies. The notations $\Gamma_i+\Gamma_j$ are abbreviated as $\Gamma_{i,j}$ in

Fig. 2(b). The tables indicate that the symmetry Γ_{dip} of the dipolar operator, which transforms like a polar vector of components $\{x, y, z\}$, is given by different symmetries, depending on the orientation of the electric field of the emitted photon: $\Gamma_1(z) + \Gamma_5(x) + \Gamma_6(y)$. Let Γ_c and Γ_v represent the representations of the conduction and valence bands, and let Γ_{env} denote the symmetry of the set of the excitonic envelope functions. The symmetry of the excitonic states are obtained, in the most general case, as the reducible product [52]:

$$\Gamma_c \otimes \Gamma_v^* \otimes \Gamma_{env} = \sum_i \Gamma_{exc}^{(i)} \tag{2}$$

In the theory of the hydrogenic atoms, *only* states $\{|n, 0, 0\rangle\}$ of the n's kind have the possibility to couple radiatively with the electromagnetic field, which in the language we use here, writes:

$$\Gamma_{env} \equiv \Gamma_1 \tag{3}$$

This equation still holds in our case although, from the cylindrical symmetry around the c axis, these are now the $\{|n, l, 0\rangle\}$ states, with l even, that have the possibility to couple radiatively with the electromagnetic field [53]. In the absence of exciton, the ground state of the crystal is also of Γ_1 symmetry. Therefore the selection rules are at the end obtained by the simple equation:

$$\Gamma_c \otimes \Gamma_v^* \otimes \Gamma_{dip} \supset \Gamma_1 \tag{4}$$

There are two main cases to consider:

1. When the polarization of the emitted photon is along the z direction, which is equivalent to $\Gamma_{dip} = \Gamma_1$, the selection rules indicate that dipolar excitonic recombinations are allowed for the specific situation when the symmetries of the conduction and valence bands are switched from Γ_7 to Γ_8 and vice versa.

2. When the polarization of the exciton is polarized in the plane orthogonal to z, two (equivalent) cases can be distinguished:

   (a) When the electric field of the emitted photon is along the x direction, which is equivalent to $\Gamma_{dip} = \Gamma_5$, dipolar excitonic recombinations are allowed for the specific situation where the symmetries of the conduction and valence bands are Γ_7 (resp. Γ_8) and Γ_7 (resp. Γ_{12}).

   (b) When the electric field of the emitted photon is along the y direction, which is equivalent to $\Gamma_{dip} = \Gamma_6$, dipolar excitonic recombinations are allowed for the specific situation where the symmetries of the conduction and valence bands are Γ_8 (resp. Γ_7) and Γ_8 (resp. Γ_{11}).

This quite abstract description can be simplified if working in the context of an angular momentum representation in a spherical space, and using the familiar notations of the textbooks of atomic physics in the context of quantum mechanics. Let as usual J_1 be the spatial angular momentum of the electron wave function and $S = 1/2$, the spin angular momentum. The total angular momentum of the electron scales from $J = J_1 + 1/2$ to $J = J_1 - 1/2$ and given a J, the series of states $|J, mj\rangle$ is $2J + 1$ times degenerated. The representation D_j that describes the symmetry of the quantum state represented by J is either irreducible or expanded along a series of irreducible representations. According to the tables of Koster *et al.* [51], in the case of the C_6 point symmetry:

- two-fold states $D_{1/2}$ $\{|1/2, \pm 1/2\rangle\}$, built from $J_1 = 0$ and $S = 1/2$, transform like $\Gamma_7 + \Gamma_8$;
- four-fold states $D_{3/2}$ $\{|3/2, \pm 3/2\rangle\}$, built from $J_1 = 1$ and $S = 1/2$, transform like $\Gamma_7 + \Gamma_8$ $\{|3/2, \pm 1/2\rangle\}$ and $\Gamma_{11} + \Gamma_{12}$ $\{|3/2, \pm 3/2\rangle\}$;
- two-fold states $D_{1/2}$ $\{|1/2, \pm 1/2\rangle\}$, built from $J_1 = 1$ and $S = 1/2$, transform like $\Gamma_7 + \Gamma_8$;
- six-fold states $D_{5/2}$ $\{|5/2, \pm 5/2\rangle\}$, built from $J_1 = 2$ and $S = 1/2$, transform like $(\Gamma_7 + \Gamma_8)\{|5/2, \pm 1/2\rangle\} + (\Gamma_{11} + \Gamma_{12})\{|5/2, \pm 3/2\rangle\} + (\Gamma_9 + \Gamma_{10})\{|5/2, \pm 5/2\rangle\})$.

Obviously the analysis of the selection rules using the representation of the symmetries of the different quantities in terms of the irreducible representations Γ_is is identical to the prescription of the selection rules for optical transitions in the context of the dipolar approximation in atomic physics: $\Delta_j = \pm 1$; $\Delta_{m_j} = 0, \pm 1$ [54]. This teaches us why transitions from $\{|5/2, \pm 5/2\rangle$ to $\{|1/2, \pm 1/2\rangle$ are forbidden. This is indicated by a distinctive color of the corresponding valence bands in Fig. 2(b). The symmetry of the second conduction band (not visible in Fig. 2(b) but in Fig. S2) is $\Gamma_9 + \Gamma_{10}$ and therefore all transitions from the VBs to this conduction band are also forbidden except from the $\Gamma_9 + \Gamma_{10}$ VB in the z polarization and from the $\Gamma_{11} + \Gamma_{12}$ VB for polarizations orthogonal to z. We disregard this possibility as

in the energy range of our experiment we should detect only one line and we measured four.

Interesting to emphasize, is the identical symmetry for quantum states of the kind $\{|J, \pm\alpha\rangle\}$ for all J of a series discriminatively inside the world of either fermions or bosons, whatever α. This is not a specific quantum effect. It rather comes from the cylindrical symmetry around the z axis and it is a general property encountered for quadratic, trigonal and hexagonal symmetries [55].

V. CONCLUSION

We demonstrate the epitaxy of high cristalline quality γ-In_2Se_3 films on (0001) oriented sapphire substrates, which reveal fine features in the optical absorption at low temperature. Clear excitonic absorption and photoluminescence emission processes are demonstrated, which fade out above 120 K in agreement with a Rydberg energy of the order of 10 meV. Three optical signatures are detected at higher energy for the first time, which are associated to direct transitions from the spin-orbit split off valence bands to the lowest conduction band which respect the selection rules of the C_6 point group. Thus on top of its ferroelectric properties the γ-polytype of In_2Se_3 owns interesting optical properties, which should motivate further experimental and theoretical research.

[1] S. A. Vitale, D. Nezich, J. O. Varghese, P. Kim, N. Gedik, P. Jarillo-Herrero, D. Xiao, and M. Rothschild, Valleytronics: Opportunities, Challenges, and Paths Forward, Small **14**, 1801483 (2018).

[2] F. Miao, S.-J. Liang, and B. Cheng, Straintronics with van der Waals materials, npj Quantum Materials **6**, 59 (2021).

[3] Z. Hennighausen and S. Kar, Twistronics: a turning point in 2D quantum materials, Electronic Structure **3**, 014004 (2021).

[4] F. Xue, J.-H. He, and X. Zhang, Emerging van der Waals ferroelectrics: Unique properties and novel devices, Applied Physics Reviews **8**, 021316 (2021).

[5] Y. Zhou, D. Wu, Y. Zhu, Y. Cho, Q. He, X. Yang, K. Herrera, Z. Chu, Y. Han, M. C. Downer, H. Peng, and K. Lai, Out-of-Plane Piezoelectricity and Ferroelectricity in Layered α-In_2Se_3 Nanoflakes, Nano Letters **17**, 5508 (2017).

[6] J. Xiao, H. Zhu, Y. Wang, W. Feng, Y. Hu, A. Dasgupta, Y. Han, Y. Wang, D. A. Muller, L. W. Martin, P. Hu, and X. Zhang, Intrinsic Two-Dimensional Ferroelectricity with Dipole Locking, Phys. Rev. Lett. **120**, 227601 (2018).

[7] F. Xue, W. Hu, K.-C. Lee, L.-S. Lu, J. Zhang, H.-L. Tang, A. Han, W.-T. Hsu, S. Tu, W.-H. Chang, C.-H. Lien, J.-H. He, Z. Zhang, L.-J. Li, and X. Zhang, Room-Temperature Ferroelectricity in Hexagonally Layered α-In_2Se_3 Nanoflakes down to the Monolayer Limit, Advanced Functional Materials **28**, 1803738 (2018).

[8] M. Küpers, P. M. Konze, A. Meledin, J. Mayer, U. Englert, M. Wuttig, and R. Dronskowski, Controlled crystal growth of indium selenide, In_2Se_3, and the crystal structures of α-In_2Se_3, Inorganic Chemistry **57**, 11775 (2018), pMID: 30153016, https://doi.org/10.1021/acs.inorgchem.8b01950.

[9] R. Rashid, F. C.-C. Ling, S.-P. Wang, K. Xiao, X. Cui, Q. Rao, and D.-K. Ki, IP and OOP ferroelectricity in hexagonal γ-In_2Se_3 nanoflakes grown by chemical vapor deposition, Journal of Alloys and Compounds **870**, 159344 (2021).

[10] M. Si, A. K. Saha, S. Gao, G. Qiu, J. Qin, Y. Duan, J. Jian, C. Niu, H. Wang, W. Wu, S. K. Gupta, and P. D. Ye, A ferroelectric semiconductor field-effect transistor, Nature Electronics **2**, 580 (2019).

[11] K. Xu, W. Jiang, X. Gao, Z. Zhao, T. Low, and W. Zhu, Optical control of ferroelectric switching and multifunctional devices based on van der Waals ferroelectric semiconductors, Nanoscale **12**, 23488 (2020).

[12] Y. Su, X. Li, M. Zhu, J. Zhang, L. You, and E. Y. Tsymbal, Van der Waals Multiferroic Tunnel Junctions, Nano Letters **21**, 175 (2021).

[13] W. Qiao, D. Jin, W. Mi, D. Wang, S. Yan, X. Xu, and T. Zhou, Large perpendicular magnetic anisotropy of transition metal dimers driven by polarization switching of two-dimensional ferroelectric In_2Se_3 substrate, arXiv:2202.13726v1 (2022).

[14] K. Dou, W. Du, Y. Dai, B. Huang, and Y. Ma, 2D magnetoelectric multiferroics in MnSTe/In_2Se_3 heterobilayer with ferroelectrically controllable skyrmions, arXiv:2202.13069v1 (2022).

[15] M. Yudasaka, T. Matsuoka, and K. Nakanishi, Indium selenide film formation by the double-source evaporation of indium and selenium, Thin Solid Films **146**, 65 (1987).

[16] G. Gordillo and C. Calderón, CIS thin film solar cells with evaporated InSe buffer layers, Solar Energy Materi-

als and Solar Cells **77**, 163 (2003).

[17] I.-H. Choi, The preparation of a $CuInSe_2$ solar cell by metal organic chemical vapor deposition, Thin Solid Films **525**, 137 (2012).

[18] C.-H. Ho and Y.-C. Chen, Thickness-tunable band gap modulation in γ-In_2Se_3, RSC Adv. **3**, 24896 (2013).

[19] A. Likforman, D. Carré, and R. Hillel, Structure cristalline du séléniure d'indium In_2Se_3, Acta Crystallographica Section B **34**, 1 (1978), https://onlinelibrary.wiley.com/doi/pdf/10.1107/S0567740878002174.

[20] S. Marsillac, J. Bernede, R. L. Ny, and A. Conan, A new simple technique to obtain In_2Se_3 polycrystalline thin films, Vacuum **46**, 1315 (1995).

[21] A. Pfitzner and H. Lutz, Redetermination of the crystal structure of γ-In_2Se_3 by twin crystal x-ray method, Journal of Solid State Chemistry **124**, 305 (1996).

[22] A. R. Barron, MOCVD of Group III Chalcogenide Compound Semiconductors, MRS Proceedings **335**, 317 (1993).

[23] P. O'Brien, D. J. Otway, and J. R. Walsh, The Growth of Indium Selenide Thin Films from a Novel Asymmetric Dialkyldiselenocarbamate of Indium, Chemical Vapor Deposition **3**, 227 (1997).

[24] K. J. Chang, S. M. Lahn, and J. Y. Chang, Growth of single-phase In_2Se_3 by using metal organic chemical vapor deposition with dual-source precursors, Applied Physics Letters **89**, 182118 (2006).

[25] R. Ma, M. D. Yang, C. H. Hu, S. C. Tong, J. L. Shen, S. M. Lan, C. H. Wu, and T. Y. Lin, Structural and optical characteristics of γ-In_2Se_3 nanorods grown on si substrates, Journal of Nanomaterials **2011**, 976262 (2011).

[26] L. Brahim-Otsmane, J.-Y. Emery, and M. Eddrief, X-ray, reflection high electron energy diffraction and x-ray photoelectron spectroscopy studies of InSe and γ-In_2Se_3 thin films grown by molecular beam deposition, Thin Solid Films **237**, 291 (1994).

[27] C. Amory, J. C. Bernède, and S. Marsillac, Study of a growth instability of γ-In_2Se_3, Journal of Applied Physics **94**, 6945 (2003).

[28] T. Okamoto, A. Yamada, and M. Konagai, Growth and characterization of In_2Se_3 epitaxial films by molecular beam epitaxy, Journal of Crystal Growth **175-176**, 1045 (1997).

[29] M. S. Claro, J. Grzonka, N. Nicoara, P. J. Ferreira, and S. Sadewasser, Wafer-scale fabrication of 2D β-In_2Se_3 photodetectors, Advanced Optical Materials **9**, 2001034 (2021).

[30] H. Lutz, M. Fischer, H.-P. Baldus, and R. Blachnik, Zur polymorphe des In_2Se_3, Journal of the Less-Common Metals **143**, 83 (1988).

[31] X. Yin, Y. Shen, C. Xu, J. He, J. Li, H. Ji, J. Wang, H. Li, X. Zhu, X. Niu, and Z. Wang, Monolithic epitaxy and optoelectronic properties of single-crystalline γ-In_2Se_3 thin films on mica, Chinese Physics B **30**, 017701 (2021).

[32] J. Thomas, N. E. Weston, and T. E. O'Connor, Turbostratic Boron Nitride, Thermal Transformation to Ordered-layer-lattice Boron Nitride, Journal of the American Chemical Society **84**, 4619 (1962).

[33] M. Moret, A. Rousseau, P. Valvin, S. Sharma, L. Souqui, H. Pedersen, H. Högberg, G. Cassabois, J. Li, J. H. Edgar, and B. Gil, Rhombohedral and turbostratic boron nitride: X-ray diffraction and photoluminescence signatures, Applied Physics Letters **119**, 262102 (2021).

[34] K. Kambas and C. Julien, Preparation and some optical and electrical measurements of a new phase α'-In_2Se_3, Materials Research Bulletin **17**, 1573 (1982).

[35] S. Marsillac, A. Combot-Marie, J. Bernède, and A. Conan, Experimental evidence of the low-temperature formation of γ-In_2Se_3 thin films obtained by a solid-state reaction, Thin Solid Films **288**, 14 (1996).

[36] M. Ueta, H. Kanzaki, K. K., Y. Toyozawa, and E. Hanamura, *Excitonic Processes in Solids*, edited by M. Cardona, P. Fulde, K. von Klitzing, and H.-J. Queisser, Vol. 60 (Springer-Verlag Berlin Heidelberg, 1986).

[37] M. Piacentini, E. Doni, R. Girlanda, V. Grasso, and A. Balzarotti, Electronic properties of the III-VI layer compounds GaS, GaSe and InSe, Il Nuovo Cimento B (1971-1996) **54**, 269 (1979).

[38] T. V. Shubina, W. Desrat, M. Moret, A. Tiberj, O. Briot, V. Y. Davydov, A. V. Platonov, M. A. Semina, and B. Gil, InSe as a case between 3D and 2D layered crystals for excitons, Nature Communications **10**, 3479 (2019).

[39] C. Klingshirn, *Semiconductor Optics* (Springer-Verlag Berlin Heidelberg 2005, 2005).

[40] J. Dillinger, Č. Koňák, V. Prosser, J. Sak, and M. Zvára, Phonon-assisted exciton transitions in $A^{II}B^{VI}$ semiconductors, physica status solidi (b) **29**, 707 (1968).

[41] R. Le Toullec, N. Piccioli, and J. C. Chervin, Optical properties of the band-edge exciton in GaSe crystals at 10 K, Phys. Rev. B **22**, 6162 (1980).

[42] B. Gil, *Physics of Wurtzite Nitrides and Oxides : Passport to Devices* (Springer Series in Materials Science, Volume 197, Springer International Publishing, 2014).

[43] B. Gil, *Group III Nitride Semiconductor Compounds: Physics and Applications* (Clarendon Press Oxford 1998, 1998).

[44] T. Ohtsuka, T. Okamoto, A. Yamada, and M. Konagai, Photoluminescence study of γ-In_2Se_3 epitaxial films grown by molecular beam epitaxy, Journal of Luminescence **87-89**, 293 (2000).

[45] Y.-C. Huang, Z.-Y. Li, W.-Y. Uen, S.-M. Lan, K. Chang, Z.-J. Xie, J. Chang, S.-C. Wang, and J.-L. Shen, Growth of γ-In_2Se_3 films on Si substrates by metal-organic chemical vapor deposition with different temperatures, Journal of Crystal Growth **310**, 1679 (2008).

[46] D. Lyu, T. Lin, T. Chang, S. Lan, T. Yang, C. Chiang, C. Chen, and H. Chiang, Structural and optical characterization of single-phase γ-In_2Se_3 films with room-temperature photoluminescence, Journal of Alloys and Compounds **499**, 104 (2010).

[47] N. Balakrishnan, E. D. Steer, E. F. Smith, Z. R. Kudrynskyi, Z. D. Kovalyuk, L. Eaves, A. Patanè, and P. H. Beton, Epitaxial growth of γ-InSe and α, β, and γ-In_2Se_3 on ϵ-GaSe, 2D Materials **5**, 035026 (2018).

[48] G. Davies, The optical properties of luminescence centres in silicon, Physics Reports **176**, 83 (1989).

[49] N. Kuroda, I. Munakata, and Y. Nishina, Exciton transitions from spin-orbit split off valence bands in layer compound InSe, Solid State Communications **33**, 687 (1980).

[50] A. Segura, J. Bouvier, M. V. Andrés, F. J. Manjón, and V. Muñoz, Strong optical nonlinearities in gallium and indium selenides related to inter-valence-band transitions induced by light pulses, Phys. Rev. B **56**, 4075 (1997).

[51] G. F. Koster, J. O. Dimmock, R. G. Wheeler, and H. Statz, *Properties of the Thirty-Two Point Groups* (MIT Press, Cambridge, MA, 1963).

[52] F. Bassani and G. Pastori Parravicini, *Electron States and Optical Transitions in Solids* (Pergamon Press, Oxford, New York, 1975).

[53] A. Baldereschi and M. Díaz, Anisotropy of excitons in semiconductors, Il Nuovo Cimento B **68**, 217 (1970).

[54] H. A. Bethe and R. W. Jackiw, *Intermediate Quantum Mechanics* (W. A. Benjamin Inc., New York, Amsterdam, 1968).

[55] J. F. Nye, *Physical Properties of Crystals: Their Representation by Tensors and Matrices* (Oxford University Press, Oxford, 1957).